HHS Public Access

Author manuscript

Nano Lett. Author manuscript; available in PMC 2023 September 14.

Published in final edited form as:

Nano Lett. 2022 September 14; 22(17): 7119–7128. doi:10.1021/acs.nanolett.2c02226.

Controlling Nanoparticle Uptake in Innate Immune Cells with Heparosan Polysaccharides

Wen Yang[1], **Alex N. Frickenstein**[1], **Vinit Sheth**[1], **Alyssa Holden**[1], **Evan M. Mettenbrink**[1], **Lin Wang**[1], **Alexis A. Woodward**[1], **Bryan S. Joo**[1], **Sarah K. Butterfield**[1], **Nathan D. Donahue**[1], **Dixy E. Green**[2], **Abigail G. Thomas**[1], **Tekena Harcourt**[1], **Hamilton Young**[1], **Mulan Tang**[1], **Zain A. Malik**[1], **Roger G. Harrison**[3], **Priyabrata Mukherjee**[4,5], **Paul L. DeAngelis**[2], **Stefan Wilhelm**[1,5,6,*]

[1]Stephenson School of Biomedical Engineering, University of Oklahoma, Norman, Oklahoma, 73019, USA

[2]Department of Biochemistry and Molecular Biology, University of Oklahoma Health Sciences Center, Oklahoma City, Oklahoma, 73104, USA

[3]School of Chemical, Biological and Materials Engineering, University of Oklahoma, Norman, Oklahoma, 73019, USA

[4]Department of Pathology, The University of Oklahoma Health Sciences Center, Oklahoma City, Oklahoma, 73104, USA

[5]Stephenson Cancer Center, University of Oklahoma Health Sciences Center, Oklahoma City, Oklahoma, 73104, USA

[6]Institute for Biomedical Engineering, Science, and Technology (IBEST), University of Oklahoma, Norman, Oklahoma, 73019, USA

Abstract

We used heparosan (HEP) polysaccharides for controlling nanoparticle delivery to innate immune cells. Our results show that HEP-coated nanoparticles were endocytosed in a time-dependent manner by innate immune cells via both clathrin-mediated and macropinocytosis pathways. Upon endocytosis, we observed HEP-coated nanoparticles in intracellular vesicles and the cytoplasm, demonstrating the potential for nanoparticle escape from intracellular vesicles. Competition with other glycosaminoglycan types inhibited the endocytosis of HEP-coated nanoparticles only partially. We further found that nanoparticle uptake into innate immune cells can be controlled by more than three orders of magnitude via systematically varying the HEP surface density. Our results suggest a substantial potential for HEP-coated nanoparticles to target innate immune cells for efficient intracellular delivery, including into the cytoplasm. This HEP nanoparticle surface engineering technology may be broadly used to develop efficient nanoscale devices for drug and gene delivery as well as gene editing and immuno-engineering applications.

*Corresponding author: Stefan Wilhelm, Ph.D., stefan.wilhelm@ou.edu.

Supporting Information

This material is available free of charge via the internet at http://pubs.acs.org. The supporting information includes supplementary figures S1–S33, and the methods and materials.

Graphical Abstract

Keywords

Heparosan; surface modification; endocytosis; nanoparticles; antigen-presenting cells; immunomodulation

Nanoparticles can deliver biomolecular and other payloads to cells of the innate immune system[1–3]. Upon entry into the body, antigen-presenting cells of the innate immune system can recognize foreign entities, such as pathogens, to elicit immune responses[3–6]. In addition, immune responses can be initiated and boosted through interactions between engineered nanoparticles and immune cells to bridge the gap between innate and adaptive immune systems[7–11]. Therefore, understanding the nanoparticles' interaction with the innate immune system is critical for developing safe and effective nanoparticle-based immunotherapeutics.

In the last decade, multiple nanoparticle surface engineering strategies have been used to target cells of the innate immune system[5,12–14]. However, the observed levels of nanoparticle uptake are not always appropriate for clinical use and may cause cellular or systemic toxicity[15,16]. There is a need to develop methods to control nanoparticle uptake into innate immune cells to elicit desired immune responses[8,13,17–20]. This approach can minimize undesirable side effects of nanomedicines, enabling the development of new nanoparticle-based applications for immunomodulation, immunotherapy, and vaccination[8,13,17–20].

We demonstrated that heparosan (HEP) is an effective surface engineering technology to create nanoparticles that exhibit reduced protein corona formation with favorable interactions with antigen-presenting cells[13]. This study investigated the interactions between HEP-modified nanoparticles and innate immune cells mechanistically by determining the nanoparticle cellular uptake characteristics and associated endocytosis pathways. Considering that nanoparticle surface properties govern cellular interactions[15,16,21–23], we investigated the nanoparticle uptake efficiency using competition assays of various HEP structural analogs, i.e. polymers of the glycosaminoglycan (GAG) family, and by systematically varying the HEP surface coating density. Our results show that nanoparticle uptake in innate immune cells can be controlled over three orders of magnitude by varying the HEP surface coating density. These findings may enable the development of safe and effective nanomedicines for applications in immunomodulation, immunotherapy, and vaccine research.

In Figure S1, we demonstrated that HEP-coated gold nanoparticles (HEP-AuNPs) efficiently target antigen-presenting cells, such as macrophages and dendritic cells, consistent with our previous findings[13]. This study used RAW 264.7 macrophages and DC 2.4 dendritic cells as model immune cells. As shown under the light micrographs in Figures 1A and S2, HEP-AuNPs exhibit a time-dependent nanoparticle uptake behavior when incubated with RAW 264.7 macrophages or DC 2.4 dendritic cells. The progressively darker cell coloration (due to the reddish AuNPs) upon brightfield imaging over time suggests an increase in nanoparticle uptake. We quantified the nanoparticle cellular uptake in RAW 264.7 (Figure 1B) and DC 2.4 (Figure S3) cells by inductively coupled plasma mass spectrometry (ICP-MS). We observed that the nanoparticle uptake per cell increased over time, plateauing at ~12 h post-incubation. These results show that innate immune cells exhibit a time-dependent cellular uptake process to internalize HEP-coated nanoparticles.

To further validate the time-dependent cellular internalization, we performed confocal laser scanning microscopy (CLSM) to monitor the nanoparticle uptake behavior in real-time in RAW 264.7 macrophages up to 7 h post-incubation (Figure 1C–D, Figure S4). The HEP-AuNPs were imaged label-free via nanoparticle light scattering and were mainly present surrounding the cell membrane after 1 h of incubation[13,24]. We observed strong intracellular nanoparticle signals at 4.5 h, 5 h, and 7 h time points post-incubation. To corroborate the intracellular and localization, we subsequently visualized the spatial distribution of nanoparticles in RAW 264.7 macrophages at 3 h, 6 h, and 24 h (Figure 1E and Figure S5) and DC 2.4 dendritic cells at 3 h and 24 h (Figure S6) post-incubation by transmission electron microscopy (TEM). We observed that the HEP-AuNPs were present in intracellular vesicles and discovered that some nanoparticles could escape from these intracellular vesicles to access the cytoplasm (Figure 1E and S7). Furthermore, we detected some HEP-nanoparticles in lysosomes after 3 h incubation by CLSM via a LysoTracker™ Deep Red staining, a red fluorescent dye that accumulates in lysosomes (Figure S8). Our findings reveal that the cellular uptake of HEP-AuNPs in RAW 264.7 macrophages and DC 2.4 dendritic cells is time-dependent, with a majority of internalized nanoparticles present in intracellular vesicles and a smaller fraction of nanoparticles accessing the cytoplasm.

Since we observed HEP-AuNPs in intracellular vesicles, we hypothesized that these nanoparticles might enter cells via endocytosis by one or more energy-dependent uptake pathways[25,26]. We carried out a systematic endocytosis inhibition study to discern which uptake pathways were involved. First, we confirmed that energy-dependent endocytosis facilitated the observed nanoparticle uptake by exposing the RAW 264.7 macrophages to known non-specific endocytosis inhibition conditions, i.e low temperature (4°C) or 0.1% w/v sodium azide [27–29]. We found that the cellular uptake of HEP-AuNPs was reduced by ~89% and ~22% when the cells were incubated with nanoparticles at 4°C (Figure 2B and Figure S9) or treated with sodium azide, respectively (Figure 2C and Figure S9), confirming an energy-dependent nanoparticle uptake process.

Next, we screened specific endocytosis pathways using established chemical inhibitors (Table 1) that more selectively block endocytosis using inhibitor concentrations from published literature (Figure 2A). First, we pre-incubated the innate immune cells for 1 h with the endocytosis inhibitors. Then we added the nanoparticles and incubated them

with the cells for 1.5 h. We imaged the cells with a light microscope and quantified the nanoparticle uptake by ICP-MS (Figure 2D and Figure S9–10). The ICP-MS results revealed that nanoparticle cellular uptake inhibition efficiencies were ~73%, 12%, 24%, or 8% for chlorpromazine, chloroquine, cytochalasin D, or imipramine, respectively (Figure 2D).

Under our study conditions, the chlorpromazine inhibitor was the most effective agent. As shown in Figures 2D and S9–10, the endocytosis inhibitors N-ethylmaleimide (NEM), Filipin, Dynasore, and 5-(*N*-ethyl-*N*-isopropyl) amiloride (EIPA) did not reduce the nanoparticle cellular uptake. It is known that the cellular uptake machinery and cellular metabolic processes are inter-connected and thus, uptake and transport mechanisms in the context of nanoparticles are difficult to completely define[30]. However, our findings suggest that HEP-AuNPs primarily enter the model innate immune cells through clathrin-mediated endocytosis and macropinocytosis pathways with some possibility of phagocytosis.

As schematically shown in Figure 3A, chlorpromazine inhibits clathrin-mediated endocytosis while cytochalasin D inhibits macropinocytosis/phygocytosis[51,53]. In our screening experiments, these agents were the most effective HEP-AuNP uptake inhibitors (Figure 2). We performed systematic dose escalation studies to assess the dose-response of the inhibitory effect and the cell toxicity of these two agents. Based on the previous dose screening experiments and published cell viability data[30,54,55], the dose ranges were 0–31.4 μM and 0–3.9 μM for chlorpromazine and cytochalasin D, respectively. The cell viability assays confirmed that these inhibitor doses were not cytotoxic under the tested conditions (Figure 3B–C). Using ICP-MS analysis, we quantified the inhibitory effects for nanoparticle uptake in RAW264.7 macrophages to be ~70% (chlorpromazine) and ~51% (cytochalasin D), respectively (Figure 3B–C). Furthermore, the cell light micrographs showed an apparent reduction in light extinction, consistent with a decrease in nanoparticle cellular uptake (Figure S11–12). The notably reduced cellular uptake levels upon chlorpromazine (23.5 μM) and Cytochalasin D (3.0 μM) incubation with RAW 264.7 macrophages were confirmed qualitatively by CLSM imaging (Figure 3D). Reduced nanoparticle intensity signals were observed in the cell groups treated with the inhibitors compared to those without the inhibitors (Figure 3D).

To test whether the HEP-coated nanoparticles could enter cells through clathrin-mediated endocytosis and macropinocytosis/phagocytosis in another immune cell line, we conducted similar inhibition experiments in DC 2.4 dendritic cells. As shown in Figure S13, both chlorpromazine and cytochalasin D reduced HEP-AuNP uptake by ~77% in DC 2.4 dendritic cells. Additionally, we co-incubated chlorpromazine and cytochalasin D inhibitors with cells to test if there was any additive endocytosis inhibitory effect. Upon co-incubation of these two inhibitors, we quantified an ~71% inhibitory effect. Thus, significant additive endocytosis inhibition was not observed with this inhibitor combination. We corroborated this finding by co-incubating RAW 264.7 macrophages with both inhibitors (Figure S14). We observed no significant cytotoxicity of the inhibitors at these tested doses (Figure S15).

To investigate the role of phagocytosis on the HEP-AuNPs cellular uptake, we conducted a systematic set of experiments involving inhibition of the process via: (i) physical saturation with 3-μm polymeric microspheres, and (ii) chemical inhibition by the compounds Cdc42/

Rac1 and NSC 23766 (Table 1) in RAW 264.7 and DC 2.4 cells. As shown in Figures S16–19, there was no significant reduction of HEP-nanoparticle cellular uptake suggesting only a potentially minor role of phagocytosis. We additionally did not observe an inhibitory effect on nanoparticle cellular uptake in RAW 264.7 upon using Annexin V (Figure S20). Our results indicate that the cell uptake of HEP-AuNPs occurs in a time-dependent facilitated primarily by clathrin-mediated endocytosis and macropinocytosis.

Our experiments showed that clathrin-mediated endocytosis plays an important role in the cellular uptake of HEP-AuNPs, indicating that specific cell surface receptors may facilitate nanoparticle cell uptake. Since these cell surface receptors are unknown, we wondered whether various structural analogs of HEP polysaccharides, the glycosaminoglycans including heparin, hyaluronan (HA), chondroitin sulfates (CS), could be used as competitors and thereby reduce the uptake of HEP-AuNPs (Figure 4A).

To address this question, we pre-incubated RAW 264.7 macrophages systematically with a library of relevant HEP structural analogs (Table 2) and then added HEP-AuNPs to the cells. To quantify the nanoparticles' cellular interactions, we performed quantitative ICP-MS (Figure 4B and Figures S21–22) and corroborated the results qualitatively with light microscopy (Figure 4C–E, Figures S21 and S23). The ICP-MS and microscopy data both revealed that CS A (i.e. CS with mostly C4-sulfo isomers) was most effective at reducing the cellular uptake (~43%) of HEP-AuNPs compared with the 'no-competitor' group. We observed ~15% inhibition by CS C (i.e. CS with mostly C6-sulfo isomers) and ~18% inhibition by heparin (i.e. the anticoagulant drug that is a highly sulfated HEP); no significant competition with the remaining structural analogs was observed (Figure 4B, Figures S21–22). Heparosan itself was not a good competitor (either the high molecular weight 169-kDa HEP or the 13-kDa HEP used for the nanoparticle coating). We speculate that the multivalent interactions of the HEP-AuNPs with cells were too strong to be effectively competed by a 'monovalent' free HEP chain.

We next investigated whether the CS A inhibitory effect of HEP-AuNP uptake was due to a potential toxicity effect of the CS A preparation, which was extracted from a mammalian source. We observed that the CS A material did not affect cell viability at the working concentrations employed in this study (Figures 4C–E, S21, S23–25).

Next, we expanded the structural analog competition study to DC 2.4 dendritic cells. Since the previous study demonstrated that CS A significantly reduced uptake of the HEP-AuNPs in RAW 264.7 macrophages, we pre-incubated CS A with the DC 2.4 cells for 1 h, then added the nanoparticles for an additional 2.5-h incubation. We quantified the competition efficiency by ICP-MS and corroborated the results with light microscopy (Figures S25–26). Non-cytotoxic doses of CS A resulted in a lower nanoparticle uptake as quantified by ICP-MS, and we observed a reduced nanoparticle signal compared to the no-competitor group using light microscopy (Figures S25–26).

We further assessed the competition effect of CS A as a function of time and concentration at non-cytotoxic levels. The CS A agent significantly lowered the cell uptake of HEP-AuNPs, as confirmed by light microscopy and ICP-MS quantification (Figures S27–30 and

Figures 4F–G). The inhibitory effect of 1 mg/mL CS A persisted throughout time (Figure 4F). At 2 mg/mL, CS A suppressed cellular uptake of HEP-AuNPs up to 9-fold, according to our inhibitor dose-response results (IC_{50} of 0.5 mg/mL, Figure 4G). These competition experiments with GAG structural analog polymers imply that CS A can substitute as a ligand for HEP for the internalization receptor(s). However, the receptor identity remains unknown.

Next, we investigated whether the observed substantial cellular uptake of HEP-AuNPs was due to multivalent nanoparticle/receptor interactions by evaluating the effect of the HEP surface coating density on internalization. Since uncoated nanoparticles are prone to colloidal instability and substantial protein corona formation that may affect cellular interactions[70–75], we first coated the nanoparticles with various amounts of HEP polymers. We then used a backfilling strategy to cover any uncoated surface with methoxy-terminated poly(ethylene glycol), PEG, thereby enhancing nanoparticle colloidal stability (Figure 5A and Figure S1). PEG is known to minimize non-specific protein adsorption on nanoparticle surfaces, and it is used in the clinic[13,76]. We characterized the coating process by measuring the hydrodynamic diameter and zeta potential with DLS. The data show that with HEP added at ≥0.5 HEP/nm^2, there was no significant difference in the hydrodynamic diameter or the zeta potential values after PEG backfilling. At the added densities of <0.5 HEP/nm^2, the hydrodynamic diameter and the zeta potential increased with the addition of PEG, indicating that the nanoparticles were successfully backfilled (Figure S31 and S33A–B). These results confirm that fully surface-coated nanoparticles with various HEP densities were generated successfully.

Next, we exposed the nanoparticles with various HEP surface coating densities to RAW 264.7 macrophages and evaluated the corresponding uptake efficiencies qualitatively by light microscopy and quantitatively by ICP-MS (Figure 5B–E and Figure S33C–D). We observed that the interaction between the nanoparticles and the cells increased in a HEP surface coating density-dependent manner using light microscopy (Figure 5C–E and Figures S32–33D). We corroborated this observation quantitatively by ICP-MS. Our quantitative results demonstrate that the nanoparticle cellular uptake can be controlled by more than three orders of magnitude via varying the HEP surface coating density (Figure 5B and Figure S33C). Overall, our results suggest that the multivalent interactions strengthen with increased HEP surface coating density, leading to higher HEP-AuNP cell uptake. Manipulating the surface HEP coating density could provide a strategy for the controlled delivery of nanoparticles to innate immune cells.

In the current work, we studied the cellular uptake behavior and endocytosis pathways of HEP-AuNPs in innate immune cells, e.g., macrophages and dendritic cells, that are antigen-presenting cells. Our results demonstrate that HEP-coated nanoparticles are endocytosed by cells in a time-dependent manner and internalized into intracellular vesicles through clathrin-mediated endocytosis and macropinocytosis. We found that some fraction of internalized nanoparticles could access the cytoplasm. The nanoparticle cellular uptake is strongly affected by the HEP surface coating density. This nanoparticle uptake can be controlled over three orders of magnitude through HEP surface coating density engineering. The ability to control the uptake of HEP-coated nanoparticles in innate immune cells

could enable the future development of safe, effective, and efficient nanoparticle-based immunotherapies and vaccines.

Supplementary Material

Refer to Web version on PubMed Central for supplementary material.

Acknowledgments

The authors thank Dr. Chen for providing the DC 2.4 dendritic cells. Additionally, the authors acknowledge the University of Oklahoma (OU) Samuel Roberts Noble Microscopy Laboratory (SRNML), the OU Mass Spectrometry, Proteomics & Metabolomics (MSPM) Core, and the Oklahoma Medical Research Foundation (OMRF) Imaging Core Facility for assistance. This work was supported in part by an NSF MRI grant (1828234), NSF CAREER award (2048130), an NIH COBRE award (P20GM135009), an IBEST/OUHSC seed grant for interdisciplinary research, the OU VPRP Strategic Equipment Investment grant, the OU Faculty Investment Program, an OCAST Health Research grant (HR20-106), Oklahoma Center for the Advancement of Science and Technology, and the Oklahoma Tobacco Settlement Endowment Trust awarded to the University of Oklahoma Stephenson Cancer Center. The content is solely the responsibility of the authors and does not necessarily represent the official views of the Oklahoma Tobacco Settlement Endowment Trust. PM acknowledges funding from NIH R01CA136494 and R01CA213278.

References

(1). Wilhelm S; Tavares AJ; Dai Q; Ohta S; Audet J; Dvorak HF; Chan WCW Analysis of Nanoparticle Delivery to Tumours. Nat Rev Mater 2016, 1 (5), 1–12. 10.1038/natrevmats.2016.14.

(2). Zhao Z; Ukidve A; Kim J; Mitragotri S Targeting Strategies for Tissue-Specific Drug Delivery. Cell 2020, 181 (1), 151–167. 10.1016/j.cell.2020.02.001. [PubMed: 32243788]

(3). Boraschi D; Italiani P; Palomba R; Decuzzi P; Duschl A; Fadeel B; Moghimi SM Nanoparticles and Innate Immunity: New Perspectives on Host Defence. Seminars in Immunology 2017, 34, 33–51. 10.1016/j.smim.2017.08.013. [PubMed: 28869063]

(4). Aroh C; Wang Z; Dobbs N; Luo M; Chen Z; Gao J; Yan N Innate Immune Activation by CGAMP-PC7A Nanoparticles Leads to Potent and Long-Acting Antiretroviral Response against HIV-1. J Immunol 2017, 199 (11), 3840–3848. 10.4049/jimmunol.1700972. [PubMed: 29084836]

(5). Liu Y; Hardie J; Zhang X; Rotello VM Effects of Engineered Nanoparticles on the Innate Immune System. Semin Immunol 2017, 34, 25–32. 10.1016/j.smim.2017.09.011. [PubMed: 28985993]

(6). La-Beck NM; Gabizon AA Nanoparticle Interactions with the Immune System: Clinical Implications for Liposome-Based Cancer Chemotherapy. Frontiers in Immunology 2017, 8, 416. [PubMed: 28428790]

(7). Donahue ND; Acar H; Wilhelm S Concepts of Nanoparticle Cellular Uptake, Intracellular Trafficking, and Kinetics in Nanomedicine. Advanced Drug Delivery Reviews 2019, 143, 68–96. 10.1016/j.addr.2019.04.008. [PubMed: 31022434]

(8). Yang W; Wang L; Mettenbrink EM; DeAngelis PL; Wilhelm S Nanoparticle Toxicology. Annu. Rev. Pharmacol. Toxicol. 2021, 61 (1), 269–289. 10.1146/annurev-pharmtox-032320-110338. [PubMed: 32841092]

(9). Beck JD; Reidenbach D; Salomon N; Sahin U; Türeci Ö; Vormehr M; Kranz LM MRNA Therapeutics in Cancer Immunotherapy. Mol Cancer 2021, 20, 69. 10.1186/s12943-021-01348-0. [PubMed: 33858437]

(10). Yin Q; Yu W; Grzeskowiak CL; Li J; Huang H; Guo J; Chen L; Wang F; Zhao F; von Boehmer L; Metzner TJ; Leppert JT; Chien Y-H; Kuo CJ; Davis MM Nanoparticle-Enabled Innate Immune Stimulation Activates Endogenous Tumor-Infiltrating T Cells with Broad Antigen Specificities. Proc Natl Acad Sci U S A 2021, 118 (21), e2016168118. 10.1073/pnas.2016168118. [PubMed: 34021082]

(11). Iwasaki A; Medzhitov R Regulation of Adaptive Immunity by the Innate Immune System. Science 2010, 327 (5963), 291–295. 10.1126/science.1183021. [PubMed: 20075244]

(12). Mizrahy S; Raz SR; Hasgaard M; Liu H; Soffer-Tsur N; Cohen K; Dvash R; Landsman-Milo D; Bremer MGEG; Moghimi SM; Peer D Hyaluronan-Coated Nanoparticles: The Influence of the Molecular Weight on CD44-Hyaluronan Interactions and on the Immune Response. Journal of Controlled Release 2011, 156 (2), 231–238. 10.1016/j.jconrel.2011.06.031. [PubMed: 21745506]

(13). Yang W; Wang L; Fang M; Sheth V; Zhang Y; Holden AM; Donahue ND; Green DE; Frickenstein AN; Mettenbrink EM; Schwemley TA; Francek ER; Haddad M; Hossen MN; Mukherjee S; Wu S; DeAngelis PL; Wilhelm S Nanoparticle Surface Engineering with Heparosan Polysaccharide Reduces Serum Protein Adsorption and Enhances Cellular Uptake. Nano Lett. 2022, 22 (5), 2103–2111. 10.1021/acs.nanolett.2c00349. [PubMed: 35166110]

(14). Liu Y; Wang L; Song Q; Ali M; Crowe WN; Kucera GL; Hawkins GA; Soker S; Thomas KW; Miller LD; Lu Y; Bellinger CR; Zhang W; Habib AA; Petty WJ; Zhao D Intrapleural Nano-Immunotherapy Promotes Innate and Adaptive Immune Responses to Enhance Anti-PD-L1 Therapy for Malignant Pleural Effusion. Nat Nanotechnol 2022, 17 (2), 206–216. 10.1038/s41565-021-01032-w. [PubMed: 34916656]

(15). Ding H; Ma Y Controlling Cellular Uptake of Nanoparticles with PH-Sensitive Polymers. Sci Rep 2013, 3 (1), 2804. 10.1038/srep02804. [PubMed: 24076598]

(16). Bai Y; Xing H; Wu P; Feng X; Hwang K; Lee JM; Phang XY; Lu Y; Zimmerman SC Chemical Control over Cellular Uptake of Organic Nanoparticles by Fine Tuning Surface Functional Groups. ACS Nano 2015, 9 (10), 10227–10236. 10.1021/acsnano.5b03909. [PubMed: 26327513]

(17). Costa da Silva M; Vieira Rocha C; Bañobre-López M; Gallo J Stimulation and Suppression of the Innate Immune System through Nanotechnology. ACS Appl. Nano Mater. 2021, 4 (3), 2303–2316. 10.1021/acsanm.0c03424.

(18). Cai J; Wang H; Wang D; Li Y Improving Cancer Vaccine Efficiency by Nanomedicine. Adv. Biosys. 2019, 3 (3), 1800287. 10.1002/adbi.201800287.

(19). van Leent MMT; Priem B; Schrijver DP; de Dreu A; Hofstraat SRJ; Zwolsman R; Beldman TJ; Netea MG; Mulder WJM Regulating Trained Immunity with Nanomedicine. Nat Rev Mater 2022, 1–17. 10.1038/s41578-021-00413-w.

(20). Moynihan KD; Opel CF; Szeto GL; Tzeng A; Zhu EF; Engreitz JM; Williams RT; Rakhra K; Zhang MH; Rothschilds AM; Kumari S; Kelly RL; Kwan BH; Abraham W; Hu K; Mehta NK; Kauke MJ; Suh H; Cochran JR; Lauffenburger DA; Wittrup KD; Irvine DJ Eradication of Large Established Tumors in Mice by Combination Immunotherapy That Engages Innate and Adaptive Immune Responses. Nat Med 2016, 22 (12), 1402–1410. 10.1038/nm.4200. [PubMed: 27775706]

(21). Verma A; Stellacci F Effect of Surface Properties on Nanoparticle-Cell Interactions. Small 2010, 6 (1), 12–21. 10.1002/smll.200901158. [PubMed: 19844908]

(22). Nel AE; Mädler L; Velegol D; Xia T; Hoek EMV; Somasundaran P; Klaessig F; Castranova V; Thompson M Understanding Biophysicochemical Interactions at the Nano–Bio Interface. Nature Mater 2009, 8 (7), 543–557. 10.1038/nmat2442. [PubMed: 19525947]

(23). Chou T, Y. L; Ming K; Chan W, C. W Strategies for the Intracellular Delivery of Nanoparticles. Chemical Society Reviews 2011, 40 (1), 233–245. 10.1039/C0CS00003E. [PubMed: 20886124]

(24). Donahue ND; Sheth V; Frickenstein AN; Holden A; Kanapilly S; Stephan C; Wilhelm S Absolute Quantification of Nanoparticle Interactions with Individual Human B Cells by Single Cell Mass Spectrometry. Nano Lett. 2022, 22 (10), 4192–4199. 10.1021/acs.nanolett.2c01037. [PubMed: 35510841]

(25). Fobian S-F; Petzer M; Vetten M; Steenkamp V; Gulumian M; Cordier W Mechanisms Facilitating the Uptake of Carboxyl–Polythene Glycol-Functionalized Gold Nanoparticles into Multicellular Spheroids. Journal of Pharmacy and Pharmacology 2022, rgac017. 10.1093/jpp/rgac017.

(26). Foroozandeh P; Aziz AA Insight into Cellular Uptake and Intracellular Trafficking of Nanoparticles. Nanoscale Research Letters 2018, 13 (1), 339. 10.1186/s11671-018-2728-6. [PubMed: 30361809]

(27). Li Y; Monteiro-Riviere NA Mechanisms of Cell Uptake, Inflammatory Potential and Protein Corona Effects with Gold Nanoparticles. Nanomedicine 2016, 11 (24), 3185–3203. 10.2217/nnm-2016-0303. [PubMed: 27882809]

(28). Gao H; Yang Z; Zhang S; Cao S; Shen S; Pang Z; Jiang X Ligand Modified Nanoparticles Increases Cell Uptake, Alters Endocytosis and Elevates Glioma Distribution and Internalization. Sci Rep 2013, 3, 2534. 10.1038/srep02534. [PubMed: 23982586]

(29). Kou L; Sun J; Zhai Y; He Z The Endocytosis and Intracellular Fate of Nanomedicines: Implication for Rational Design. Asian Journal of Pharmaceutical Sciences 2013, 8 (1), 1–10. 10.1016/j.ajps.2013.07.001.

(30). Francia V; Reker-Smit C; Boel G; Salvati A Limits and Challenges in Using Transport Inhibitors to Characterize How Nano-Sized Drug Carriers Enter Cells. Nanomedicine 2019, 14 (12), 1533–1549. 10.2217/nnm-2018-0446. [PubMed: 31208280]

(31). Reisman BJ; Guo H; Ramsey HE; Wright MT; Reinfeld BI; Ferrell PB; Sulikowski GA; Rathmell WK; Savona MR; Plate L; Rubinstein JL; Bachmann BO Apoptolidin Family Glycomacrolides Target Leukemia through Inhibition of ATP Synthase. Nat Chem Biol 2022, 18 (4), 360–367. 10.1038/s41589-021-00900-9. [PubMed: 34857958]

(32). Delrot S; Despeghel J-P; Bonnemain J-L Phloem Loading in Vicia Faba Leaves: Effect of N-Ethylmaleimide and Parachloromercuribenzenesulfonic Acid on H+ Extrusion, K+ and Sucrose Uptake. Planta 1980, 149 (2), 144–148. 10.1007/BF00380875. [PubMed: 24306245]

(33). Li T; Takeoka S Enhanced Cellular Uptake of Maleimide-Modified Liposomes via Thiol-Mediated Transport. IJN 2014, 9 (1), 2849–2861. 10.2147/IJN.S58540. [PubMed: 24940060]

(34). Wenge B; Bönisch H N-Ethylmaleimide Differentially Inhibits Substrate Uptake by and Ligand Binding to the Noradrenaline Transporter. Naunyn-Schmied Arch Pharmacol 2008, 377 (3), 255–265. 10.1007/s00210-008-0272-0.

(35). Zhang H; Ding A; Ye B; Wang Z; Zhang J; Qiu L; Chen J Carbon Nitride Nanosheets for Imaging Traceable CpG Oligodeoxynucleotide Delivery. ACS Appl. Nano Mater. 2021, 4 (8), 8546–8555. 10.1021/acsanm.1c01658.

(36). Di Marzio L; Marianecci C; Cinque B; Nazzarri M; Cimini AM; Cristiano L; Cifone MG; Alhaique F; Carafa M PH-Sensitive Non-Phospholipid Vesicle and Macrophage-like Cells: Binding, Uptake and Endocytotic Pathway. Biochimica et Biophysica Acta (BBA) - Biomembranes 2008, 1778 (12), 2749–2756. 10.1016/j.bbamem.2008.07.029. [PubMed: 18762164]

(37). Wolfram J; Nizzero S; Liu H; Li F; Zhang G; Li Z; Shen H; Blanco E; Ferrari M A Chloroquine-Induced Macrophage-Preconditioning Strategy for Improved Nanodelivery. Sci Rep 2017, 7 (1), 13738. 10.1038/s41598-017-14221-2. [PubMed: 29062065]

(38). Perry JW; Wobus CE Endocytosis of Murine Norovirus 1 into Murine Macrophages Is Dependent on Dynamin II and Cholesterol. J Virol 2010, 84 (12), 6163–6176. 10.1128/JVI.00331-10. [PubMed: 20375172]

(39). Kapetanovic R; Nahori M-A; Balloy V; Fitting C; Philpott DJ; Cavaillon J-M; Adib-Conquy M Contribution of Phagocytosis and Intracellular Sensing for Cytokine Production by Staphylococcus Aureus-Activated Macrophages. Infect Immun 2007, 75 (2), 830–837. 10.1128/IAI.01199-06. [PubMed: 17118979]

(40). Lim EY; Park J; Kim YT; Kim MJ Imipramine Inhibits Migration and Invasion in Metastatic Castration-Resistant Prostate Cancer PC-3 Cells via AKT-Mediated NF-KB Signaling Pathway. Molecules 2020, 25 (20), 4619. 10.3390/molecules25204619.

(41). Almeida M. S. de; Susnik E; Drasler B; Taladriz-Blanco P; Petri-Fink A; Rothen-Rutishauser B Understanding Nanoparticle Endocytosis to Improve Targeting Strategies in Nanomedicine. Chemical Society Reviews 2021, 50 (9), 5397–5434. 10.1039/D0CS01127D. [PubMed: 33666625]

(42). Lee DJ; Cox D; Li J; Greenberg S Rac1 and Cdc42 Are Required for Phagocytosis, but Not NF-KB-Dependent Gene Expression, in Macrophages Challenged with Pseudomonas Aeruginosa *. Journal of Biological Chemistry 2000, 275 (1), 141–146. 10.1074/jbc.275.1.141. [PubMed: 10617597]

(43). Fc Receptor-Mediated Phagocytosis Requires CDC42 and Rac1. The EMBO Journal 1998, 17 (21), 6219–6229. 10.1093/emboj/17.21.6219. [PubMed: 9799231]

(44). Qu L; Wang Y; Li Y; Wang X; Li N; Ge S; Wang J; Wang G-J; Volkow ND; Lang B; Wang P; Wu H; Zeng J; Fu J; Li J; Zhang Y; Wang X Decreased Neuronal Excitability in

Medial Prefrontal Cortex during Morphine Withdrawal Is Associated with Enhanced SK Channel Activity and Upregulation of Small GTPase Rac1. Theranostics 2020, 10 (16), 7369–7383. 10.7150/thno.44893. [PubMed: 32641997]

(45). Jaynes JM; Sable R; Ronzetti M; Bautista W; Knotts Z; Abisoye-Ogunniyan A; Li D; Calvo R; Dashnyam M; Singh A; Guerin T; White J; Ravichandran S; Kumar P; Talsania K; Chen V; Ghebremedhin A; Karanam B; Bin Salam A; Amin R; Odzorig T; Aiken T; Nguyen V; Bian Y; Zarif JC; de Groot AE; Mehta M; Fan L; Hu X; Simeonov A; Pate N; Abu-Asab M; Ferrer M; Southall N; Ock C-Y; Zhao Y; Lopez H; Kozlov S; de Val N; Yates CC; Baljinnyam B; Marugan J; Rudloff U Mannose Receptor (CD206) Activation in Tumor-Associated Macrophages Enhances Adaptive and Innate Antitumor Immune Responses. Science Translational Medicine 2020, 12 (530), eaax6337. 10.1126/scitranslmed.aax6337. [PubMed: 32051227]

(46). Zhu S; Lu P; Liu H; Chen P; Wu Y; Wang Y; Sun H; Zhang X; Xia Q; Heng BC; Zhou Y; Ouyang HW Inhibition of Rac1 Activity by Controlled Release of NSC23766 from Chitosan Microspheres Effectively Ameliorates Osteoarthritis Development in Vivo. Ann Rheum Dis 2015, 74 (1), 285–293. 10.1136/annrheumdis-2013-203901. [PubMed: 24257023]

(47). Jay SM; Skokos EA; Zeng J; Knox K; Kyriakides TR Macrophage Fusion Leading to Foreign Body Giant Cell Formation Persists under Phagocytic Stimulation by Microspheres in in Vitro and in Vivo in Mouse Models. J Biomed Mater Res A 2010, 93 (1), 189–199. 10.1002/jbm.a.32513. [PubMed: 19536825]

(48). Bennett MR; Gibson DF; Schwartz SM; Tait JF Binding and Phagocytosis of Apoptotic Vascular Smooth Muscle Cells Is Mediated in Part by Exposure of Phosphatidylserine. Circ Res 1995, 77 (6), 1136–1142. 10.1161/01.res.77.6.1136. [PubMed: 7586226]

(49). van Genderen HO; Kenis H; Hofstra L; Narula J; Reutelingsperger CPM Extracellular Annexin A5: Functions of Phosphatidylserine-Binding and Two-Dimensional Crystallization. Biochimica et Biophysica Acta (BBA) - Molecular Cell Research 2008, 1783 (6), 953–963. 10.1016/j.bbamcr.2008.01.030. [PubMed: 18334229]

(50). Yoshida S; Minematsu N; Chubachi S; Nakamura H; Miyazaki M; Tsuduki K; Takahashi S; Miyasho T; Iwabuchi T; Takamiya R; Tateno H; Mouded M; Shapiro SD; Asano K; Betsuyaku T Annexin V Decreases PS-Mediated Macrophage Efferocytosis and Deteriorates Elastase-Induced Pulmonary Emphysema in Mice. Am J Physiol Lung Cell Mol Physiol 2012, 303 (10), L852–860. 10.1152/ajplung.00066.2012. [PubMed: 22962014]

(51). Sheth V; Wang L; Bhattacharya R; Mukherjee P; Wilhelm S Strategies for Delivering Nanoparticles across Tumor Blood Vessels. Adv. Funct. Mater. 2021, 31 (8), 2007363. 10.1002/adfm.202007363.

(52). Rennick JJ; Johnston APR; Parton RG Key Principles and Methods for Studying the Endocytosis of Biological and Nanoparticle Therapeutics. Nat. Nanotechnol. 2021, 16 (3), 266–276. 10.1038/s41565-021-00858-8. [PubMed: 33712737]

(53). Hossen Md. N.; Wang L; Chinthalapally HR; Robertson JD; Fung K-M; Wilhelm S; Bieniasz M; Bhattacharya R; Mukherjee P Switching the Intracellular Pathway and Enhancing the Therapeutic Efficacy of Small Interfering RNA by Auroliposome. Science Advances 2020, 6 (30), eaba5379. 10.1126/sciadv.aba5379. [PubMed: 32743073]

(54). Tian T; Zhu Y-L; Zhou Y-Y; Liang G-F; Wang Y-Y; Hu F-H; Xiao Z-D Exosome Uptake through Clathrin-Mediated Endocytosis and Macropinocytosis and Mediating MiR-21 Delivery. J Biol Chem 2014, 289 (32), 22258–22267. 10.1074/jbc.M114.588046. [PubMed: 24951588]

(55). Biddeci G; Spinelli G; Massaro M; Riela S; Bonaccorsi P; Barattucci A; Di Blasi F Study of Uptake Mechanisms of Halloysite Nanotubes in Different Cell Lines. Int J Nanomedicine 2021, 16, 4755–4768. 10.2147/IJN.S303816. [PubMed: 34285481]

(56). Rippe M; Stefanello TF; Kaplum V; Britta EA; Garcia FP; Poirot R; Companhoni MVP; Nakamura CV; Szarpak-Jankowska A; Auzély-Velty R Heparosan as a Potential Alternative to Hyaluronic Acid for the Design of Biopolymer-Based Nanovectors for Anticancer Therapy. Biomater. Sci. 2019, 7 (7), 2850–2860. 10.1039/C9BM00443B. [PubMed: 31070204]

(57). Jackson DG Hyaluronan in the Lymphatics: The Key Role of the Hyaluronan Receptor LYVE-1 in Leucocyte Trafficking. Matrix Biol 2019, 78–79, 219–235. 10.1016/j.matbio.2018.02.001.

(58). Essentials of Glycobiology, 3rd ed.; Varki A, Cummings RD, Esko JD, Stanley P, Hart GW, Aebi M, Darvill AG, Kinoshita T, Packer NH, Prestegard JH, Schnaar RL, Seeberger PH, Eds.; Cold Spring Harbor Laboratory Press: Cold Spring Harbor (NY), 2015.

(59). Chavaroche AAE; van den Broek LAM; Eggink G Production Methods for Heparosan, a Precursor of Heparin and Heparan Sulfate. Carbohydrate Polymers 2013, 93 (1), 38–47. 10.1016/j.carbpol.2012.04.046. [PubMed: 23465899]

(60). Nikitovic D; Assouti M; Sifaki M; Katonis P; Krasagakis K; Karamanos NK; Tzanakakis GN Chondroitin Sulfate and Heparan Sulfate-Containing Proteoglycans Are Both Partners and Targets of Basic Fibroblast Growth Factor-Mediated Proliferation in Human Metastatic Melanoma Cell Lines. The International Journal of Biochemistry & Cell Biology 2008, 40 (1), 72–83. 10.1016/j.biocel.2007.06.019. [PubMed: 17706452]

(61). de Vet ECJM; Newland SAB; Lyons PA; Aguado B; Campbell RD The Cell Surface Receptor G6b, a Member of the Immunoglobulin Superfamily, Binds Heparin. FEBS Letters 2005, 579 (11), 2355–2358. 10.1016/j.febslet.2005.03.032. [PubMed: 15848171]

(62). DeAngelis PL Heparosan, a Promising 'Naturally Good' Polymeric Conjugating Vehicle for Delivery of Injectable Therapeutics. Expert Opinion on Drug Delivery 2015, 12 (3), 349–352. 10.1517/17425247.2015.978282. [PubMed: 25363378]

(63). Soares da Costa D; Reis RL; Pashkuleva I Sulfation of Glycosaminoglycans and Its Implications in Human Health and Disorders. Annual Review of Biomedical Engineering 2017, 19 (1), 1–26. 10.1146/annurev-bioeng-071516-044610.

(64). Natural and Synthetic Biomedical Polymers, First edition.; Kumbar S, Laurencin C, Deng M, Eds.; Elsevier: Amsterdam ; Boston, 2014, 71–73.

(65). Fujimoto T; Kawashima H; Tanaka T; Hirose M; Toyama-Sorimachi N; Matsuzawa Y; Miyasaka M CD44 Binds a Chondroitin Sulfate Proteoglycan, Aggrecan. Int Immunol 2001, 13 (3), 359–366. 10.1093/intimm/13.3.359. [PubMed: 11222505]

(66). Hirose J; Kawashima H; Swope Willis M; Springer TA; Hasegawa H; Yoshie O; Miyasaka M Chondroitin Sulfate B Exerts Its Inhibitory Effect on Secondary Lymphoid Tissue Chemokine (SLC) by Binding to the C-Terminus of SLC. Biochim Biophys Acta 2002, 1571 (3), 219–224. 10.1016/s0304-4165(02)00232-5. [PubMed: 12090936]

(67). Zhang Q; Du Y; Chen J; Xu G; Yu T; Hua X; Zhang J Investigation of Chondroitin Sulfate D and Chondroitin Sulfate E as Novel Chiral Selectors in Capillary Electrophoresis. Anal Bioanal Chem 2014, 406 (5), 1557–1566. 10.1007/s00216-013-7544-3. [PubMed: 24363112]

(68). Mikami T; Yasunaga D; Kitagawa H Contactin-1 Is a Functional Receptor for Neuroregulatory Chondroitin Sulfate-E*. Journal of Biological Chemistry 2009, 284 (7), 4494–4499. 10.1074/jbc.M809227200. [PubMed: 19075012]

(69). Singh B; Maharjan S; Kim Y-K; Jiang T; Islam MA; Kang S-K; Cho M-H; Choi Y-J; Cho C-S Targeted Gene Delivery via N-Acetylglucosamine Receptor Mediated Endocytosis. J Nanosci Nanotechnol 2014, 14 (11), 8356–8364. 10.1166/jnn.2014.9919. [PubMed: 25958528]

(70). Sindhwani S; Syed AM; Ngai J; Kingston BR; Maiorino L; Rothschild J; MacMillan P; Zhang Y; Rajesh NU; Hoang T; Wu JLY; Wilhelm S; Zilman A; Gadde S; Sulaiman A; Ouyang B; Lin Z; Wang L; Egeblad M; Chan WCW The Entry of Nanoparticles into Solid Tumours. Nat. Mater. 2020, 19 (5), 566–575. 10.1038/s41563-019-0566-2. [PubMed: 31932672]

(71). Dai Q; Wilhelm S; Ding D; Syed AM; Sindhwani S; Zhang Y; Chen YY; MacMillan P; Chan WCW Quantifying the Ligand-Coated Nanoparticle Delivery to Cancer Cells in Solid Tumors. ACS Nano 2018, 12 (8), 8423–8435. 10.1021/acsnano.8b03900. [PubMed: 30016073]

(72). Wilhelm S; Hirsch T; Patterson WM; Scheucher E; Mayr T; Wolfbeis OS Multicolor Upconversion Nanoparticles for Protein Conjugation. Theranostics 2013, 3 (4), 239–248. 10.7150/thno.5113. [PubMed: 23606910]

(73). Donahue ND; Francek ER; Kiyotake E; Thomas EE; Yang W; Wang L; Detamore MS; Wilhelm S Assessing Nanoparticle Colloidal Stability with Single-Particle Inductively Coupled Plasma Mass Spectrometry (SP-ICP-MS). Anal Bioanal Chem 2020, 412 (22), 5205–5216. 10.1007/s00216-020-02783-6. [PubMed: 32627086]

(74). Narum SM; Le T; Le DP; Lee JC; Donahue ND; Yang W; Wilhelm S Chapter 4 - Passive Targeting in Nanomedicine: Fundamental Concepts, Body Interactions, and Clinical Potential. In

Nanoparticles for Biomedical Applications; Chung EJ, Leon L, Rinaldi C, Eds.; Micro and Nano Technologies; Elsevier, 2020; pp 37–53. 10.1016/B978-0-12-816662-8.00004-7.

(75). Lee JC; Donahue ND; Mao AS; Karim A; Komarneni M; Thomas EE; Francek ER; Yang W; Wilhelm S Exploring Maleimide-Based Nanoparticle Surface Engineering to Control Cellular Interactions. ACS Appl. Nano Mater. 2020, 3 (3), 2421–2429. 10.1021/acsanm.9b02541.

(76). Suk JS; Xu Q; Kim N; Hanes J; Ensign LM PEGylation as a Strategy for Improving Nanoparticle-Based Drug and Gene Delivery. Adv Drug Deliv Rev 2016, 99 (Pt A), 28–51. 10.1016/j.addr.2015.09.012. [PubMed: 26456916]

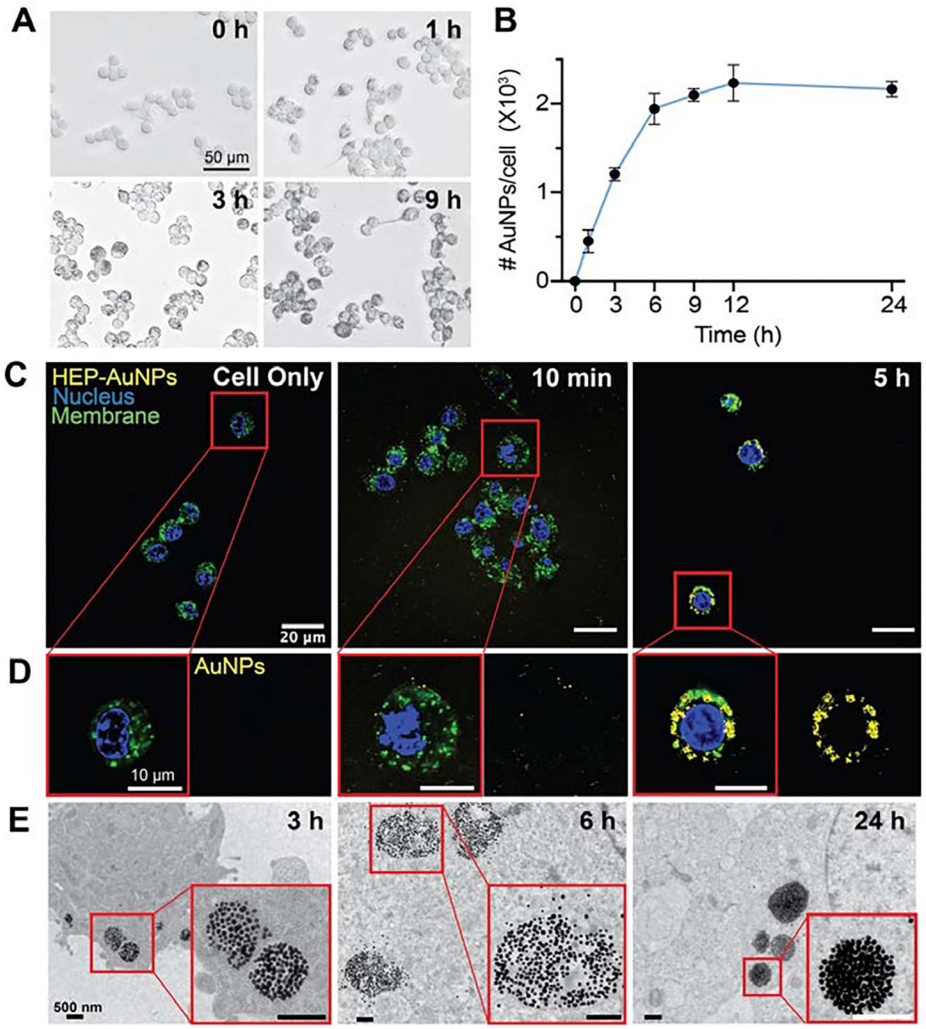

Figure 1: The cellular uptake of heparosan (HEP) modified gold nanoparticles (AuNPs) is time-dependent.

(A) Representative brightfield light micrographs of HEP-AuNPs internalization in RAW 264.7 macrophages at 0 h, 1 h, 3 h, and 9 h. Scale bar: 50 μm. (B) ICP-MS results of 55-nm HEP-AuNPs uptake in RAW 264.7 macrophages over time. The data points indicate mean values and standard deviation (n=3–4). (C) Real-time confocal laser scanning microscopy (CLSM) imaging of HEP-AuNP internalization in live RAW 264.7 macrophages. Scale bars: 20 μm. (D) A representative individual cell image was selected from panel C. The right panel shows the AuNPs channel. Scale bars: 10 μm. (E) Transmission electron micrographs of 55-nm HEP-AuNP internalization in RAW 264.7 after 3 h, 6 h, and 24 h incubation. The insert at the bottom right corner of each micrograph shows a higher magnification view of the selected field of view sections. Scale bars: 500 nm.

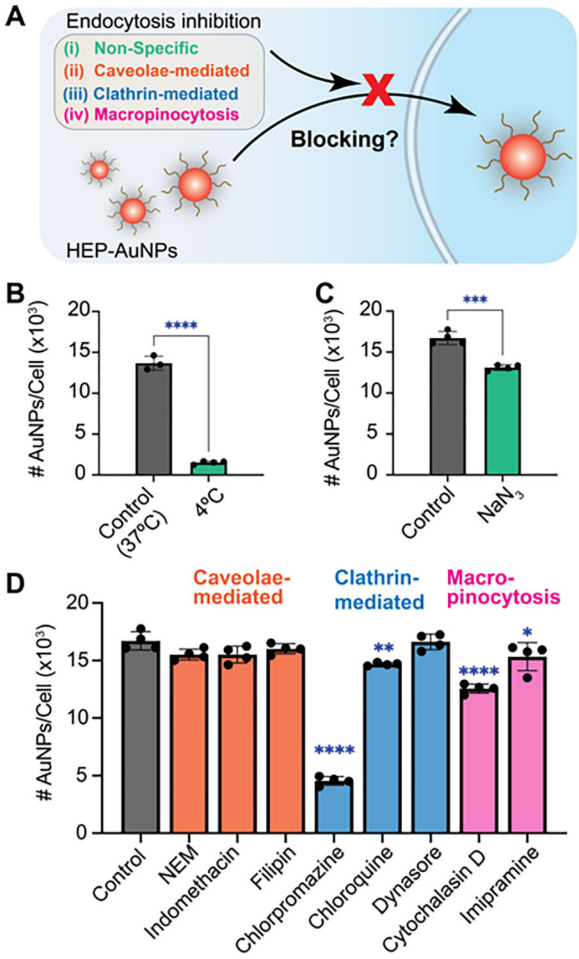

Figure 2: HEP-coated nanoparticles enter innate immune cells through endocytosis.

(A) Schematic representation of the uptake pathway study: (i) non-specific endocytosis inhibition to determine whether nanoparticle cellular uptake is energy-dependent. (ii-iv) Specific endocytosis inhibitors for studying (ii) caveolae-mediated endocytosis, (iii) clathrin-mediated endocytosis, and (iv) macropinocytosis. (B-D) ICP-MS quantification of the nanoparticle cellular uptake in RAW 264.7 macrophages at 4°C (B), in the presence of ATPase inhibitor sodium azide (C), or chemical endocytosis inhibitors of caveolae-mediated endocytosis, clathrin-mediated endocytosis, and macropinocytosis (D). AuNPs modified with 13-kDa HEP (at 0.2 nM) were used as control without inhibitors at 37°C. Bars indicate mean ± SD (n=3–4); statistical tests used one-way ANOVA ($p<0.0001$ (****); $p<0.0021$ (**); $p<0.0332$ (*).

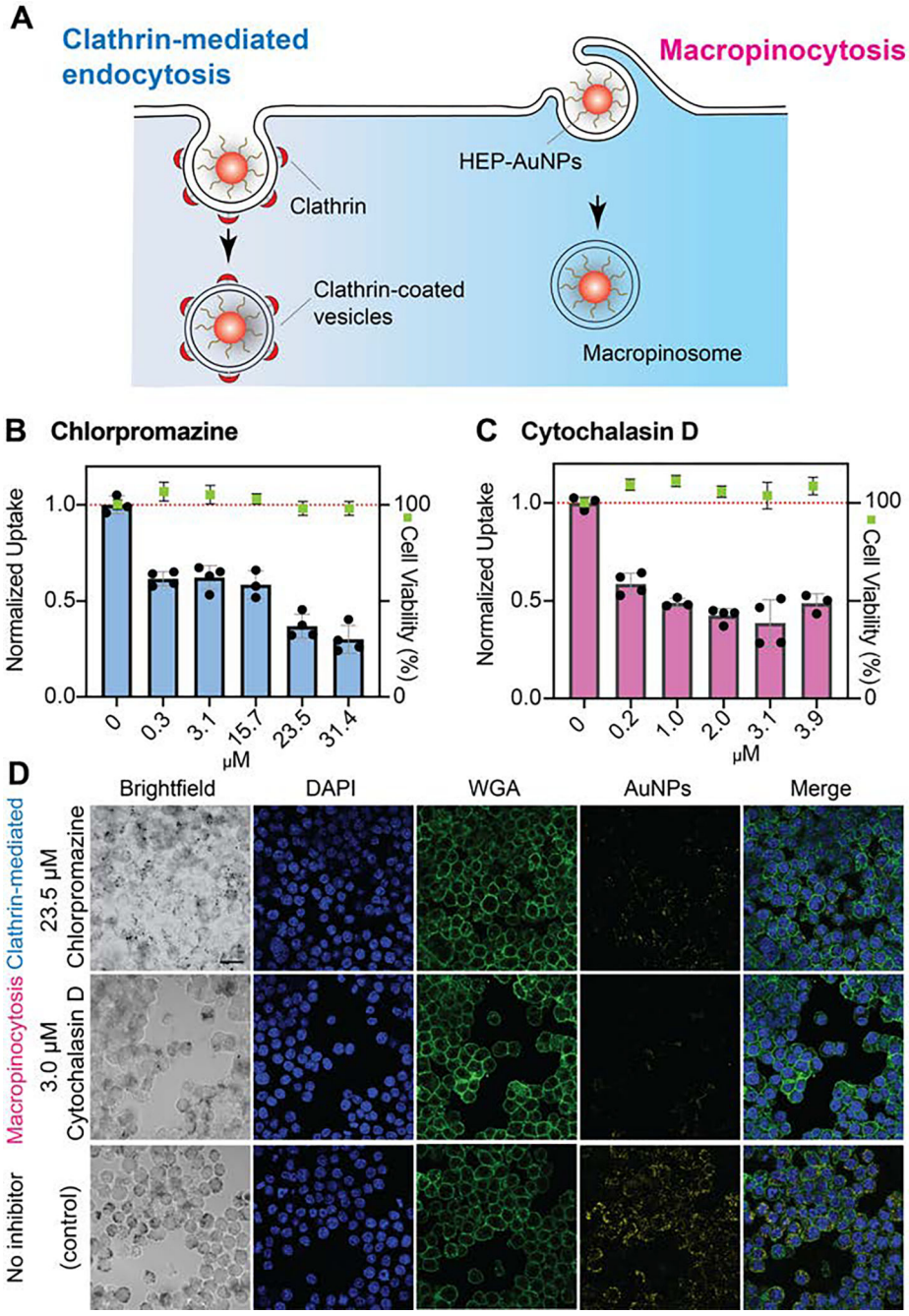

Figure 3: HEP-coated nanoparticles enter cells primarily through clathrin-mediated endocytosis and macropinocytosis.

(A) Schematic representation of HEP-AuNPs uptake through clathrin-mediated endocytosis or macropinocytosis. (B-C) ICP-MS was used to quantify the nanoparticle cellular uptake in RAW 264.7 macrophages upon inhibition with different concentrations of chlorpromazine (B; clathrin-mediated endocytosis) and cytochalasin D (C; macropinocytosis). Bars indicate mean values ± SD (n=3–4). The statistical analysis of groups with competitors showed $p<0.0001$ compared to the no-competitor group using one-way ANOVA. (D) Confocal

laser scanning micrographs of nanoparticle uptake in the presence of endocytosis inhibitors chlorpromazine or cytochalasin D along with non-inhibition control. Scale bar: 20 μm.

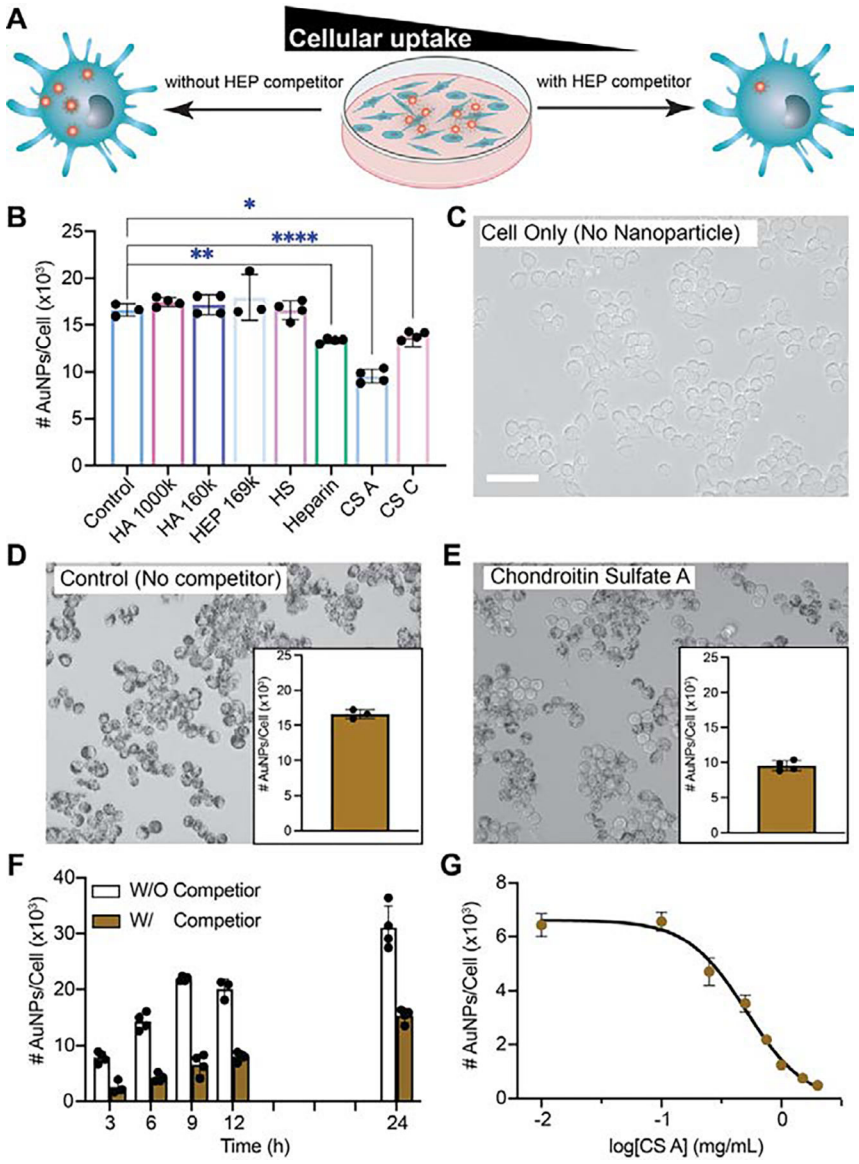

Figure 4: Evaluation of structural HEP analog polymers as competitors for HEP-coated nanoparticle uptake.

(A) Schematic illustration of the experimental design. (B) ICP-MS was used to quantify the cellular uptake of HEP-AuNPs in the presence of HEP structural analogs: 0.1 mg/mL 1,000-kDa HA, 160-kDa HA, 169-kDa HEP, heparin sulfate (HS), or heparin, and 1 mg/mL chondroitin sulfate A (CS A) or chondroitin sulfate C (CS C). The bars indicate mean values ± SD (n=3–4). Statistical tests were performed using one-way ANOVA ($p<0.0001$ (****); $p<0.0021$ (**); $p<0.0332$ (*); n.s. indicates no statistically significant differences). (C-E) Representative brightfield light micrographs of HEP-AuNPs cell uptake in the presence of competitors. The inserted bar graphs represent the quantitative ICP-MS results. The bars indicate mean values ± SD (n=3–4). Scale bar: 50 μm. (F-G) ICP-MS was used to quantify the CS A competition efficiency to reduce HEP-AuNPs cellular uptake over time (F; 1 mg/mL CS A was used) and various CS A concentrations (G). The graphs indicate mean values ± SD (n=3–4).

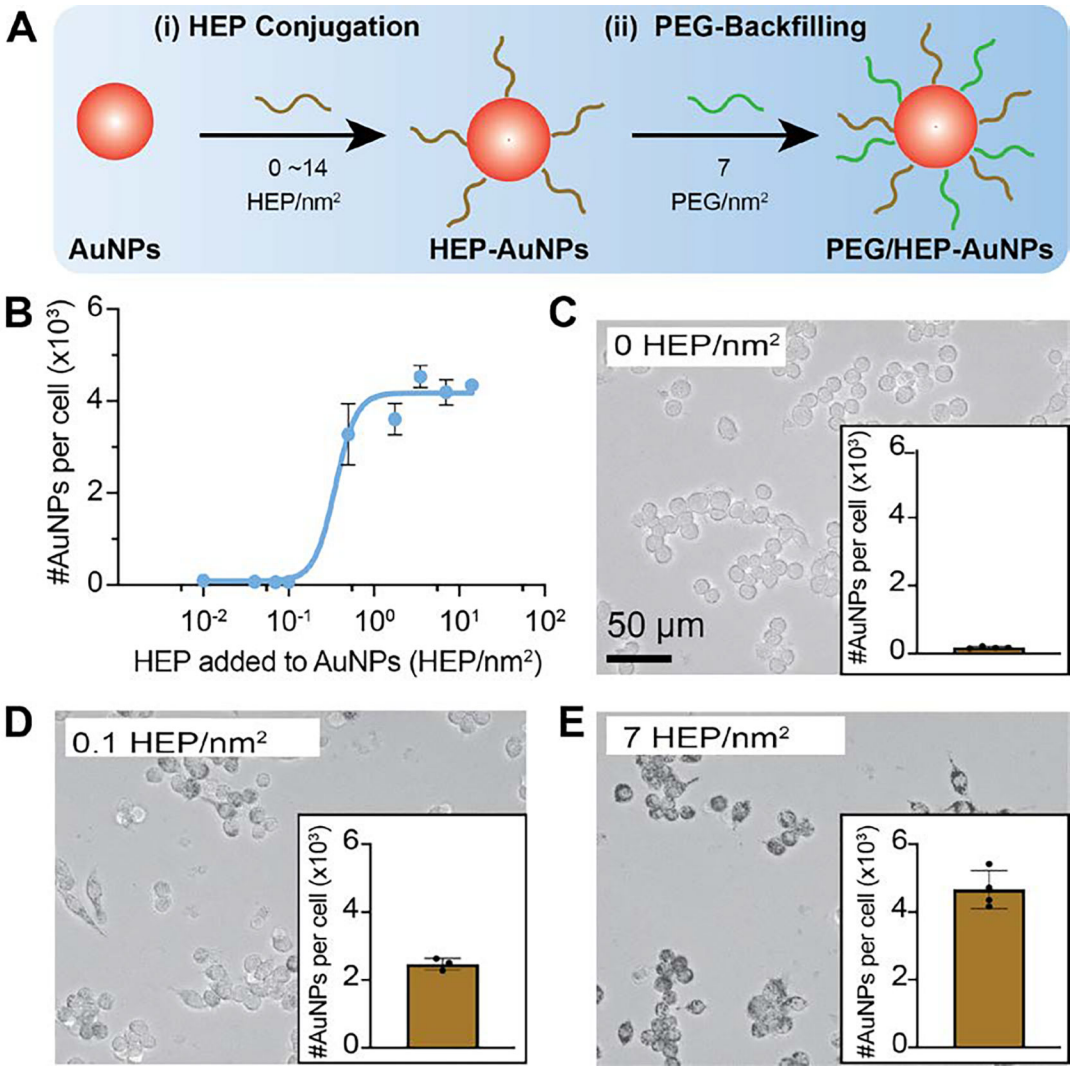

Figure 5: Nanoparticle surface coating with HEP promotes multivalent interactions with innate immune cells.

(A) Schematic representation of the surface coating process. (i) The HEP polymers were added to the AuNPs with theoretical surface coating densities ranging from 0 to 14 HEP/nm^2. (ii) Backfilling of the nanoparticle surface was achieved by adding a constant saturating amount of PEG (adding the equivalent of 7 PEG/nm^2) to generate HEP/PEG-AuNPs. (B) The uptake efficiency was measured as a function of surface HEP density by ICP-MS. The data points indicate mean values ± SD (n=3–4). (C-E) Representative brightfield light micrographs of HEP/PEG-AuNPs in cells. The dark spots within cells indicate nanoparticle accumulation. The inserted bar graphs display the quantitative ICP-MS results of nanoparticle cell uptake. The data points indicate mean values ± SD (n=3–4). Scale bar: 50 μm.

Table 1:

Summary of Endocytosis Inhibition Conditions used this Study.

Inhibitor	Mechanism of Action*	Function/Pathway*	Condition/Concentration	Ref.
Low temperature	Lowers metabolism	Non-specific endocytosis	4°C	27
Sodium Azide (NaN_3)	Decreases ATP by inhibiting glycolysis	Non-specific endocytosis	0.1% w/v	31
N-ethylmaleimide (NEM)	Inactivates the ATPase	Caveolae-mediated endocytosis	0.3 μg/mL	32–34
Indomethacin	Increases [arachidonate] to prevent plasmalemmal vesicle formation	Caveolae-mediated and clathrin-dependent endocytosis	10 μg/mL	35
Filipin	Removes cholesterol from the plasma membrane	Caveolae-mediated and clathrin-independent endocytosis	5 μg/mL	36
Chlorpromazine (CPZ)	Unknown (AP2 inhibition?)	Clathrin-mediated endocytosis	10 μg/mL	35,36
Chloroquine	Rho GTPase inhibition	Clathrin-mediated endocytosis	30 μg/mL	37
Dynasore	Blocks GTPase activity of dynamin	Clathrin-mediated endocytosis	25 μg/mL	38
Cytochalasin D (CD)	Depolymerizes F-actin	Macropinocytosis and phagocytosis	1 μg/mL	38,39
Imipramine	Inhibits the ruffling of plasma membranes	Macropinocytosis	10 μg/mL	40
Amiloride (EIPA)	Inhibits Na^+ channels and Na^+/H^+ exchange, F-action reorganization, pseudopodia retraction	Macropinocytosis and phagocytosis	10 or 20 μg/mL	41
Cdc42/Rac1	Inhibits Cdc42 and Rac1 involved regulation of actin cytoskeleton organization	Phagocytosis	1.2 – 40 μg/mL	42,43
NSC23766	Inhibits the activity of Rac1	Phagocytosis	1.6 – 106 μg/mL	44–46
3-μm Polymeric Microspheres	Saturation of phagocytosis capacity	Phagocytosis	Microsphere to cell ratio of 20:1	47
Annexin V	Masks exposed phosphatidylserine	Phagocytosis	750 μg/mL	48–50

*Information on the mechanisms of action and functions/pathways was adopted in part from reviews by Sheth et al., Rennick et al., and Almeida et al. 41,51,52.

Table 2:

Summary of HEP Structural Analog Polymers used for Competition Experiments in this Study.

GAG or Sugar	Average Molecular Weight (kDa)	Surface Receptors (not all inclusive)	Major Repeat Structure	Similarity with Heparosan	Difference from Heparosan	Ref
Heparosan	43.8; 169		[GlcA]-4-beta-[GlcNAc]-4-alpha	-	-	
Hyaluronic acid (HA)	160; 1,000	CD 44; LYVE-1; HARE; Stabilin-1	[GlcA]-3-beta-[GlcNAc]-4-beta	same sugar composition and charge density	different glycosidic linkages	56–58
Heparan Sulfate	~12.9	Fibroblast growth factor receptor	[GlcA]-[6OS-GlcNAc/GlcNS]	same backbone	~1–2 sulfates per repeat	59,60
Heparin	~16.6	G6b; Fibroblast growth factor receptor; FGF2	[2S-IdoA/GlcA]-[6OS-GlcNS]	similar backbone	~3 sulfates per repeat; some GlcA epimer, IdoA	58,59,61,62
Chondroitin Sulfate A (CS A)	~19.5	CD 44	[GlcA]-3-beta-[4S-GalNAc]-4-beta	GAG family	GalNAc instead of GlcNAc; different glycosidic linkages; 1 sulfate per repeat.	59,60,63–65
Chondroitin Sulfate B (CS B)	~21		[2S-GlcA/IdoA]-3-beta-[4,6S-GalNAc]-4-beta	GAG family	GalNAc instead of GlcNAc; different glycosidic linkages; ~2 sulfates per repeat.	66
Chondroitin Sulfate C (CS C)	~45	CD 44	[GlcA]-3-beta-[6S-GalNAc]-4-beta	GAG family	GalNAc instead of GlcNAc; different glycosidic linkages; 1 sulfate per repeat.	2
Chondroitin Sulfate D (CS D)	~39		[2S-GlcA]-3-beta-[6S-GalNAc]-4-beta	GAG family	GalNAc instead of GlcNAc; different glycosidic linkages; ~2 sulfates per repeat.	67
Chondroitin Sulfate E (CS E)	~140	Contactin-1	[GlcA]-3-beta-[4,6S-GalNAc]-4-beta	GAG family	GalNAc instead of GlcNAc; different glycosidic linkages; ~2 sulfates per repeat.	67,68
Unsulfated chondroitin	~100–200		[GlcA]-3-beta-[GalNAc]-4-beta	GAG family; same charge density	GalNAc instead of GlcNAc	
GlcNAc(*N*-acetyl-glucosamine)	0.221	-	-	monosaccharide component	-	69